




# Soft magnetic properties and loss performance of Co<sub>2</sub>O<sub>3</sub>-doped power MnZn ferrite at 100–300 kHz

Bin Fu<sup>1,2</sup>, Yaohua Yi<sup>1</sup>, Ziyu Li<sup>1</sup> , Zhong Yu<sup>1,\*</sup>, Chuanjian Wu<sup>1</sup>, Ke Sun<sup>1</sup>, Xiaona Jiang<sup>1</sup>, Qifan Li<sup>1</sup>, and Zhongwen Lan<sup>1</sup>

<sup>1</sup>School of Materials and Energy, University of Electronic Science and Technology of China, Chengdu 610054, China

<sup>2</sup>A-Core Jiangmen Electronics Company Limited, Jiangmen 529080, China

Received: 3 February 2023

Accepted: 14 May 2023

Published online:  
31 May 2023

© The Author(s), under exclusive licence to Springer Science+Business Media, LLC, part of Springer Nature 2023

## ABSTRACT

In this study, a Co<sub>2</sub>O<sub>3</sub> addition from 0.28 to 0.44 wt% is added to the MnZn ferrites. The effects of Co<sub>2</sub>O<sub>3</sub> on the soft magnetic properties and loss performance of the MnZn ferrites were investigated over a wide temperature range from 25 to 140 °C. Either the spinel crystal structure or microstructure of the MnZn ferrites is not greatly affected by the Co<sub>2</sub>O<sub>3</sub> content. The saturation magnetic induction ( $B_s$ ) shows a maximum of 528 mT at 0.36 wt% Co<sub>2</sub>O<sub>3</sub> due to the slight increase in density. At room temperature, the initial permeability ( $\mu_i$ ) of the MnZn ferrite is enhanced to a maximum of 2692, which is associated with the minimum magnetic anisotropy ( $|K|$ ) obtained at 0.36 wt% Co<sub>2</sub>O<sub>3</sub>. However, the DC resistivity of the MnZn ferrite is seen to decrease with increasing Co<sub>2</sub>O<sub>3</sub> content. Due to the enhanced initial permeability, the minimum core loss of the MnZn ferrite is obtained at 0.36 wt% Co<sub>2</sub>O<sub>3</sub> under various conditions from 100 kHz/200mT to 300 kHz/100mT.

## 1 Introduction

With the development of the third-generation semiconductor such as GaN, both the voltage and power of the switched mode power supplies (SMPS) in electronic devices have been significantly increased [1]. The MnZn ferrites are often used as the core materials in the SMPS, due to their high saturation magnetic induction ( $B_s$ ) and high initial permeability ( $\mu_i$ ). The high  $B_s$  allows for a high power density that matches the high voltage provided by the third-generation semiconductors [2]. A high  $B_s$  also results in a reduced size of magnetic core so that the device could

be made smaller. The high  $\mu_i$  facilitates the magnetization process so that a lower external magnetic field is required for the same magnetic induction.

The MnZn ferrites are known to have a composition of MO·Fe<sub>2</sub>O<sub>3</sub> with a spinel crystal structure. The tetrahedral sites (A sites) and octahedral sites (B sites) are occupied by metallic ions such as Mn<sup>2+</sup>, Fe<sup>2+</sup>, and Fe<sup>3+</sup>. Instead of being directly coupled, the metallic ions with magnetic moments are coupled by the super-exchange interactions through the non-magnetic oxygen ions. And the magnetic moment per unit cell as well as the other magnetic and electrical properties are mainly determined by the interaction

Address correspondence to E-mail: yuzhong@uestc.edu.cn

between the magnetic ions [3]. By modifying the ions distributed in A sites and B sites, the soft magnetic properties of the MnZn ferrites can be greatly affected. For example, to enhance the initial permeability of the MnZn ferrite, a Fe-rich composition is often adopted so that  $\text{Fe}^{2+}$  ions are induced to the B sites, resulting in a reduced intrinsic magnetocrystalline anisotropy constant ( $K_1$ ). Moreover, the sintering process of a Fe-rich MnZn ferrite involves a protective atmosphere with a low oxygen partial pressure to maintain a high ratio of  $\text{Fe}^{2+}$ :  $\text{Fe}^{3+}$  [4–8].

The improvement in soft magnetic properties of MnZn ferrites can also be achieved by using additives. Sintering aids such as  $\text{Bi}_2\text{O}_3$  [9–12],  $\text{MoO}_3$  [13–15], and  $\text{V}_2\text{O}_5$  [7, 16, 17] can be used to promote densification and grain growth through liquification during the sintering process. The enhanced sintering process results in a lower porosity and a larger average grain size, which are beneficial for domain wall movement in the magnetization process, leading to a higher initial permeability [3, 18–20]. Other research shows that additives such as barium titanate (BTO) and barium strontium titanate (BST) can reduce the average grain size of the MnZn ferrites and enhance the overall resistivity, resulting in significant reduction in the eddy current loss [8, 21]. Apart from additives that improves the magnetic properties only through modification of the microstructure, some metallic oxides contain ions that could enter the spinel lattices of the MnZn ferrite and affect its magnetic properties intrinsically. In this study, the effect of  $\text{Co}_2\text{O}_3$  doping on the soft magnetic properties and power loss of MnZn ferrites are investigated over a wide temperature range of 25–40 °C.

## 2 Materials and methods

The MnZn ferrites with a  $\text{Co}_2\text{O}_3$  addition from 0.28 to 0.44 wt% were prepared using the conventional ceramic method. Raw materials of  $\text{Mn}_3\text{O}_4$ , ZnO, and  $\text{Fe}_2\text{O}_3$  with an analytical grade were weighed according to the stoichiometric composition of  $\text{Mn}_{0.71}\text{Zn}_{0.22}\text{Fe}_{2.07}\text{O}_4$ . The raw materials were mixed and milled in a planetary mill at 241 rpm for 2 h with steel balls and deionized water. The mass ratio of powder:water:ball was 2:3:6. The milled powder mixture was then dried in an oven at 90 °C. Then the mixture was pre-sintered at 900 °C in air for 2 h.

After that,  $\text{Co}_2\text{O}_3$  with an analytical grade was added to the mixture from 0.28 to 0.44 wt%. The mixture was ball-milled the second time at 241 rpm/min for 3 h. The powder mixture was dried again and mixed with 12.5 wt% of polyvinyl alcohol (PVA) and granulated. The granular powder was then pressed under a pressure of 98 MPa into green bodies in the shapes of disc and chip. The green body was sintered at 1250 °C under a nitrogen atmosphere with an oxygen pressure of 3.1% for 7 h.

The crystal structure of the sintered ferrites was characterized using a MAXima XRD-7000 X-ray diffractometer (XRD). The radiation source is Cu K-alpha. The microstructure of the sintered ferrite was characterized using the JEOL JSM-6490LV scanning electron microscope (SEM) on the fractured surface of the sample. The density of the sample was measured using the Archimedeian method. The initial permeability and the DC-resistivity was measured using the TongHui TH2826 LCR meter. The magnetization curve of the sample was obtained using the LakeShore 8694 vibrating sample magnetometer (VSM). The saturation magnetization at 1200 A/m and the core loss under various conditions were measured using the IWATSU SY-8232 *B-H* analyzer.

## 3 Results and discussions

Figure 1 shows the XRD spectrum of sintered MnZn ferrites with various amount of  $\text{Co}_2\text{O}_3$  addition from 0.28 to 0.44 wt%. In reference to the standard PDF#74-2401 card, all the samples show a spinel structure without discernible sign of other crystal structure. Moreover, discernible peak splitting at higher angles (55°–70°) can be observed. This is due to the nature of K-alpha emission. As the K-alpha emission is composed of two spectral emissions, K-alpha<sub>1</sub> (wavelength,  $\lambda = 1.54060 \text{ \AA}$ ) and K-alpha<sub>2</sub> ( $\lambda = 1.54443 \text{ \AA}$ ), the latter of which have a slightly lower energy than the former, resulting in a difference in wavelength. For a given crystal structure, the relation between wavelength,  $\lambda$ , is shown in the Bragg's law:

$$n\lambda = 2d\sin\theta$$

where  $n$  is the diffraction order,  $d$  is the interplane distance, and  $\theta$  is the angle of diffraction. It is seen that peak position is directly affected by the wavelength. The mismatch of peak positions, as a result

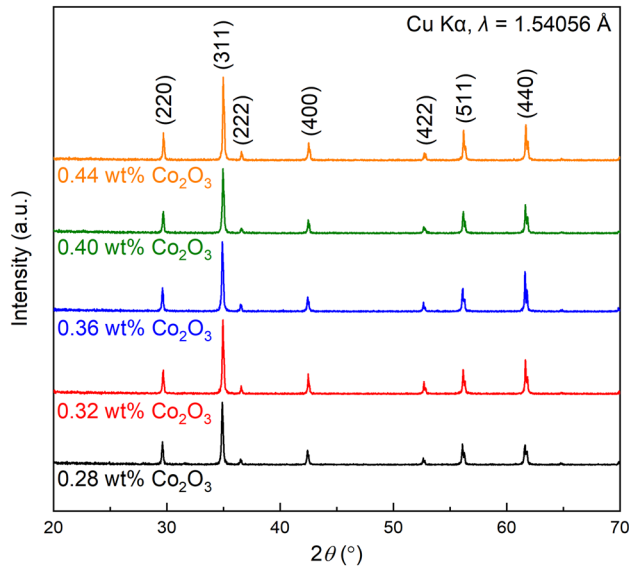


**Fig. 1** The X-ray diffraction (XRD) patterns of the MnZn ferrites with a  $\text{Co}_2\text{O}_3$  addition from 0.28 to 0.44 wt%

from the difference of  $\lambda$  between  $\text{K}\alpha_1$  and  $\text{K}\alpha_2$ , cannot be seen at lower diffraction angles, but becomes more significant at higher angles.

Figure 2 shows the morphology as well as the grain size distribution of the MnZn ferrite at the selected area on the fractured surface. Closed pores are seen at the grain boundaries as well as the joint of the grains. Figure 2b shows a normal distribution of grain size for each sample. For MnZn ferrites with a  $\text{Co}_2\text{O}_3$  addition from 0.28 to 0.44 wt%, an average grain size ranging from 8.1 to 9.1  $\mu\text{m}$  is obtained with a standard deviation from 3.7 to 4.7  $\mu\text{m}$ . It can be concluded that the  $\text{Co}_2\text{O}_3$  addition from 0.28 to 0.44 wt% has no significant effect on the microstructure. Previous studies also show a minor influence of  $\text{Co}_2\text{O}_3$  addition on the MnZn ferrites. This is natural because the  $\text{Co}^{3+}$  ions tend to diffuse into the spinel lattice without concentration difference between grains and the grain boundaries [22].

Figure 3 shows the density and the  $B_s$  of the MnZn ferrite with a  $\text{Co}_2\text{O}_3$  content of 0.28–0.44 wt%. The density of the MnZn ferrites is seen to increase slightly from 4.76  $\text{g}/\text{cm}^3$  to a maximum at 4.81  $\text{g}/\text{cm}^3$  as the  $\text{Co}_2\text{O}_3$  content is increased from 0.28 to 0.36 wt%, while the  $B_s$  is also seen to increase from 518 mT to a maximum at 528 mT. The trend of  $B_s$  changing with  $\text{Co}_2\text{O}_3$  content corresponds to that of the density. By definition,  $B_s$  is proportional to both density and the saturation magnetization,  $M_s$ . Therefore, the consistency in  $B_s$  and density changing

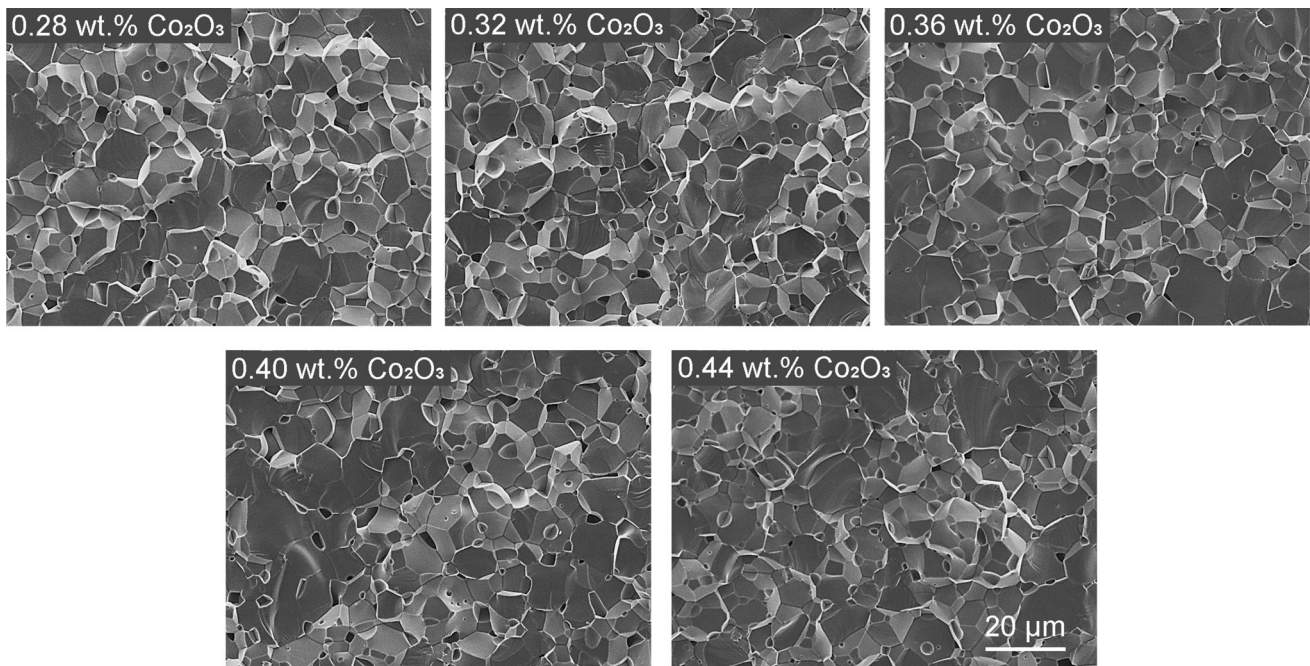
with  $\text{Co}_2\text{O}_3$  content indicates that the influence of  $\text{Co}_2\text{O}_3$  on the MnZn ferrite is minor. In the previous study by Yang and Wang [22], it is argued that  $\text{Co}^{2+}$  ions enter the octahedral sites (B-sites) of the spinel structure, replacing the  $\text{Fe}^{3+}$  and  $\text{Fe}^{2+}$  and resulting in promoted super-exchange interactions between A-sites and B-sites. The stronger super-exchange interaction between A-sites and B-sites should lead to higher net magnetic moment:  $M = M_A - M_B$ . As a result, both  $M_s$  and  $B_s$  are enhanced [22]. Yet, no further evidence was shown.

Figure 4a shows the  $B$ - $H$  of the MnZn ferrites with various amount of  $\text{Co}_2\text{O}_3$  additions. While all the samples show a narrow  $B$ - $H$  loop, samples with a  $\text{Co}_2\text{O}_3$  addition of 0.36 and 0.44 wt% have a wider  $B$ - $H$  loop. Figure 4b shows the initial permeability changing with the  $\text{Co}_2\text{O}_3$  content at 25 °C. The  $\mu_i$  is seen to increase from 2412 to 2691 as the  $\text{Co}_2\text{O}_3$  content is increased from 0.28 to 0.36 wt%, before decreasing to below 2000 as  $\text{Co}_2\text{O}_3$  content is further increased to 0.44 wt%. The  $\mu_i$  is determined by multiple factors, and can be described in the empirical relation:

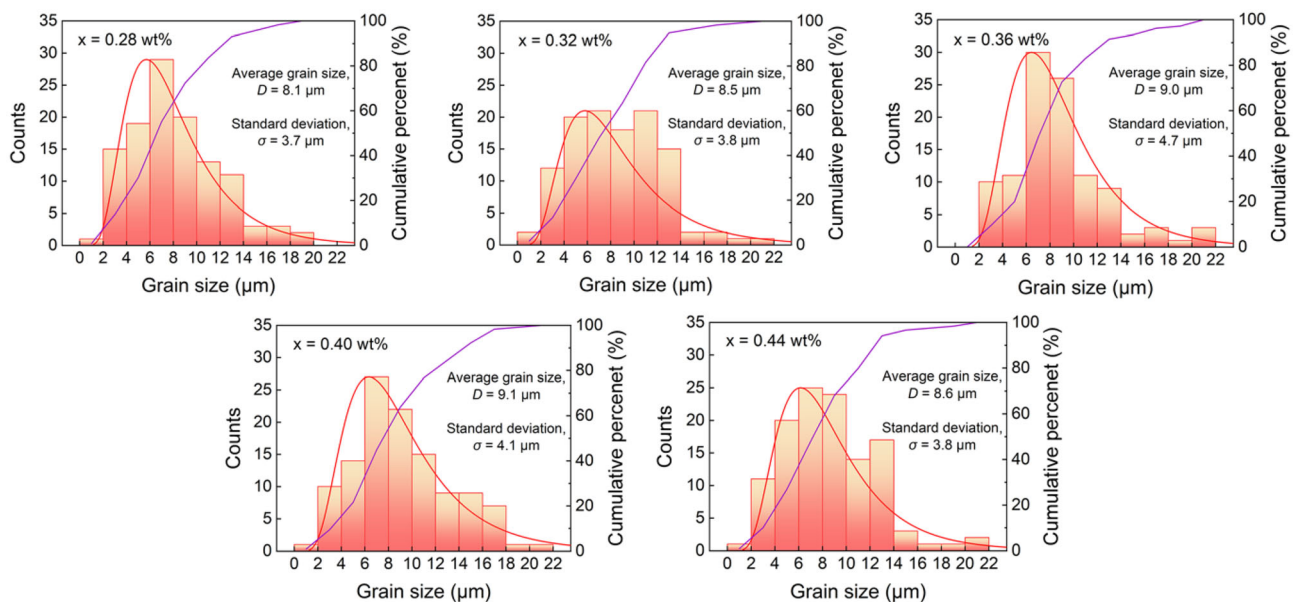
$$\mu_i \propto \frac{M_s^2}{[K_1 + 3/2\lambda_s\sigma]\beta^{1/3}\frac{\delta}{d}}$$

where  $\lambda_s$  is the saturation magnetostriction,  $\sigma$  is the internal stress,  $\delta$  is the domain wall thickness,  $\beta$  and  $d$  are the volume fraction and diameter of the impurities, respectively [23, 24]. As discussed above, the change of  $M_s$  in MnZn ferrites in this study is minor, so  $M_s$  is not considered as a primary factor causing the change in  $\mu_i$ . Instead, the major reason could be the change in the magnetocrystalline anisotropy. According to previous study, the MnZn ferrite with a composition of  $\text{Mn}_{0.71}\text{Zn}_{0.22}\text{Fe}_{2.07}\text{O}_4$  is known to possess a negative  $K_1$  value [25], and the addition of  $\text{Co}_2\text{O}_3$  is known to induce  $\text{Co}^{2+}$  ions with a positive  $K_1$  to the spinel structure and compensate the negative  $K_1$  of the original composition [26–28]. The change of magnetocrystalline anisotropy is studied and discussed later in this study.

Figure 5 shows the temperature dependence of  $\mu_i$  of the MnZn ferrites. Two peaks of the maximum  $\mu_i$  (60–80 °C and around 230 °C) can be observed, corresponding to the compensation point of magnetocrystalline anisotropy constant ( $K_1$ ) as the temperature is increased [25, 26]. At both compensation temperatures,  $\mu_i$  of the MnZn ferrites is seen to



(a)



(b)

**Fig. 2** **a** The scanning electron microscopy (SEM) images and **b** the grain size distribution of the MnZn ferrites with a Co<sub>2</sub>O<sub>3</sub> addition from 0.28 to 0.44 wt% at the fractured surface

be reduced by the Co<sub>2</sub>O<sub>3</sub> additions. Meanwhile, the first peak of  $\mu_i$  shift towards the lower temperature range and are broadened as the Co<sub>2</sub>O<sub>3</sub> addition exceeds 0.36 wt%. The peak broadening effect could also be explained by the positive magnetic anisotropy induced by Co<sup>2+</sup> [26, 29, 30] as the temperature curve of the  $\mu_i$  of MnZn ferrite become less steep. The

broadened  $\mu_i$  peak provides stability and consistency in the real-world application of MnZn ferrites where the operating temperature fluctuates.

Figure 6 shows the magnetization curve of the MnZn ferrites at room temperature obtained using the VSM. The minor fluctuation at the maximum magnetization is attributed to the change in sample

density. According to the previous research, the absolute value of  $K_1$  can be determined using the law of approach to saturation [31, 32] described in the following:

$$M(H) = M_s \left( 1 - \frac{a}{H} - \frac{b}{H^2} \right) + \chi H$$

where  $a$  and  $b$  are numerical factors representing the resistance of domain rotation,  $\chi$  represents the paramagnetic susceptibility. While  $a$  represents the influence of inhomogeneous distribution of stress and impurity,  $b$  is directly associated with the influence of magnetic anisotropy ( $K$ ):

$$b = \frac{8}{105} \frac{K^2}{\mu_0^2 M_s^2}$$

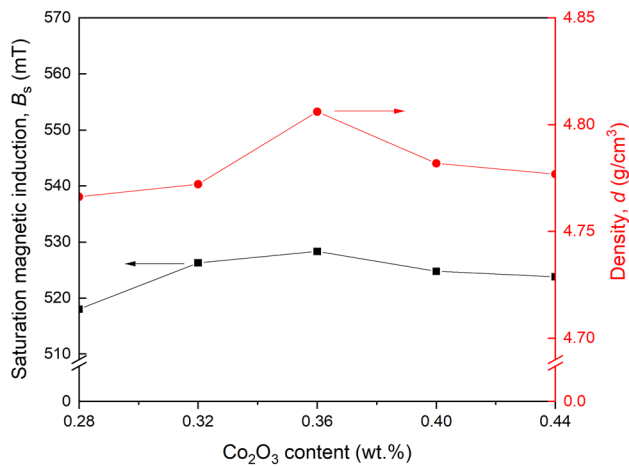


**Fig. 3** The density and saturation magnetic induction ( $B_s$ ) of the MnZn ferrites with a  $\text{Co}_2\text{O}_3$  addition of 0.28–0.44 wt%

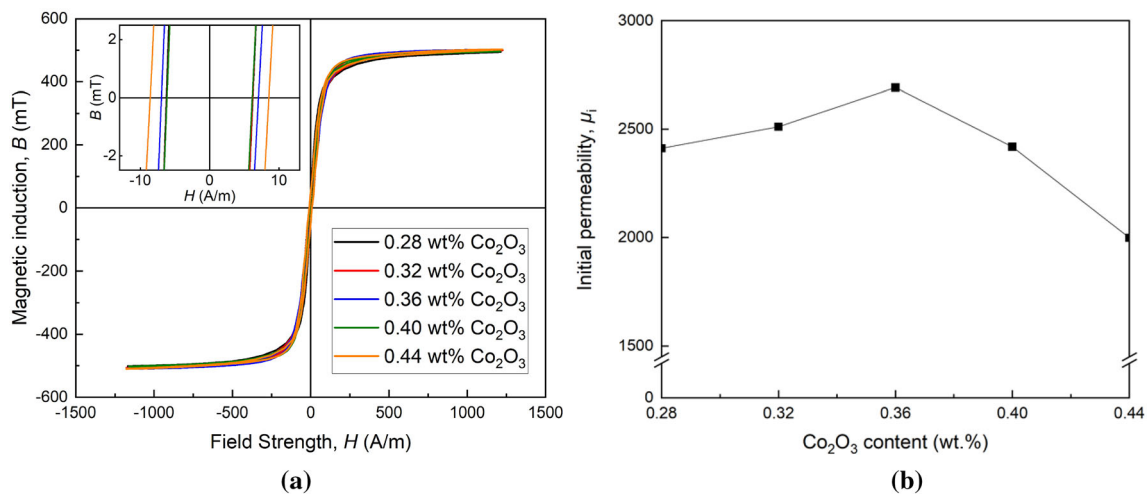


**Fig. 4** **a** The  $B$ - $H$  curves and **b** the initial permeability ( $\mu_i$ ) of the MnZn ferrite with various  $\text{Co}_2\text{O}_3$  content at room temperature

Because the influence of  $a$  is often negligible, linear fitting can be applied to the  $M(H)-1/H^2$  curve. Since the samples were prepared in the shape of a sphere, a demagnetizing factor of  $1/3$  was applied to correct the magnetization curves before fitting the data [33]. The calculated results of  $|K|$  are shown Table 1. As the  $\text{Co}_2\text{O}_3$  addition is increased from 0.28 to 0.36 wt%,  $|K|$  is reduced from  $2.47 \times 10^4 \text{ J/m}^3$  to a minimum of  $1.69 \times 10^4 \text{ J/m}^3$ . This reduction in  $|K|$  can be attributed to the compensating effect of  $\text{Co}^{2+}$  ions brought to the negative value of  $K_1$  of the MnZn ferrites [26]. As the  $\text{Co}_2\text{O}_3$  content exceeds 0.36 wt%, the value of  $K_1$  becomes positive and continue to increase, leading to the increase of the value of the overall magnetic anisotropy. The trend of  $|K|$  changing with  $\text{Co}_2\text{O}_3$  content corresponds to that of  $\mu_i$  shown in Fig. 4b, and the minimum of  $|K|$  explains for the maximum  $\mu_i$  at 0.36 wt%  $\text{Co}_2\text{O}_3$ .

Figure 7a shows the DC resistivity ( $\rho$ ) at room temperature. As the  $\text{Co}_2\text{O}_3$  content is increased from 0.28 to 0.32 wt%,  $\rho$  of the MnZn ferrites is seen to increase slightly from 11.7 to 13.1  $\Omega \text{ m}$ . However, as  $\text{Co}_2\text{O}_3$  is further increased to 0.44 wt%,  $\rho$  starts to decrease monotonously to 8.2  $\Omega \text{ m}$ . It is widely known that the relatively low resistivity of MnZn ferrites can be attributed to the hopping mechanism between  $\text{Fe}^{2+}$  and  $\text{Fe}^{3+}$  ions. According to the previous studies [22, 34], the  $\text{Co}^{3+}$  ions enter the spinel lattices and occupy the octahedral sites, where  $\text{Fe}^{2+}$  ions exist. The  $\text{Co}^{3+}$  and  $\text{Fe}^{2+}$  ions have the tendency to form  $\text{Fe}^{2+}-\text{Co}^{3+}$  pairs:

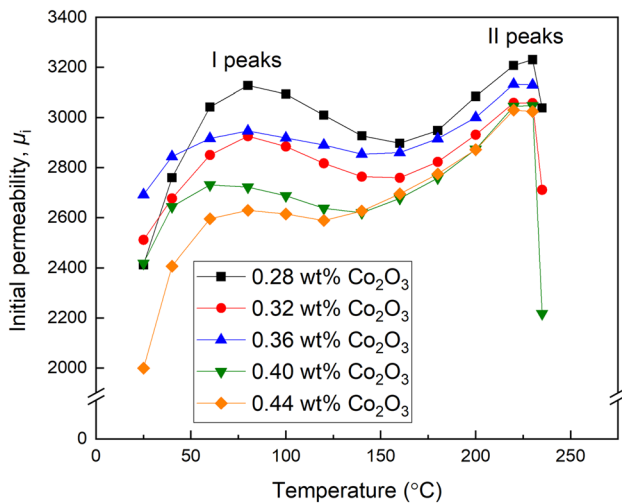


**Fig. 5** The temperature dependence of initial permeability ( $\mu_i$ ) the MnZn ferrites with various  $\text{Co}_2\text{O}_3$  content

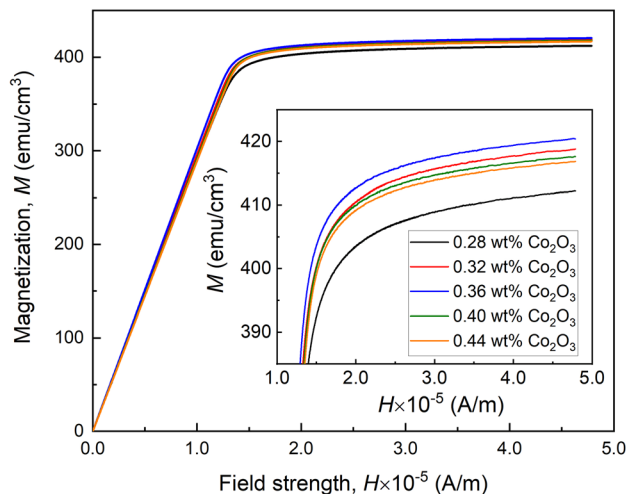
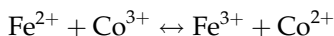


**Fig. 6** The magnetization curves of the MnZn ferrites at room temperature obtained using VSM



With the electrons from  $\text{Fe}^{2+}$  ions constrained to the  $\text{Co}^{3+}$  ions, the electron hopping between  $\text{Fe}^{2+}$  and  $\text{Fe}^{3+}$  ions is therefore limited, leading to the increased resistivity seen at the 0.32 wt%  $\text{Co}_2\text{O}_3$ . However, as the  $\text{Co}_2\text{O}_3$  content further increases, the electron hopping between the  $\text{Fe}^{2+}$ – $\text{Co}^{3+}$  pairs becomes dominant. Therefore, the resistivity starts decreasing with increasing  $\text{Co}_2\text{O}_3$  content. Figure 7b shows the temperature dependence of  $\rho$  of the MnZn ferrites with various  $\text{Co}_2\text{O}_3$  content. As the temperature is increased from 25 to 140 °C, the resistivity of the MnZn ferrites is reduced. This is due to the

**Table 1** The absolute value of magnetic anisotropy ( $|K|$ ) of the MnZn ferrites with a  $\text{Co}_2\text{O}_3$  addition from 0.28 wt% to 0.44 wt%

$\text{Co}_2\text{O}_3$ content (wt%)	0.28	0.32	0.36	0.40	0.44
$ K $ ( $\text{J}/\text{m}^3$ ) $\times 10^3$	24.71	20.95	16.85	23.18	24.03

semiconducting nature of the MnZn ferrites, where increased temperature thermally excites the electrons and enhances their mobility [35, 36]. Meanwhile, the relationship between  $\rho$  and  $\text{Co}_2\text{O}_3$  content is relatively consistent.

Figure 8 (a) shows the  $P_{\text{cv}}$  of the MnZn ferrites at 100 kHz/200mT, 200 kHz/125mT, and 300 kHz/100mT. At the above operating conditions, the contribution of hysteresis loss ( $P_{\text{h}}$ ) and eddy current loss ( $P_{\text{e}}$ ) is comparable [21]. As the  $\text{Co}_2\text{O}_3$  is increased from 0.28 to 0.36 wt%,  $P_{\text{cv}}$  at the three operating conditions is reduced to the minimum. The reduction in  $P_{\text{cv}}$  with the increasing  $\text{Co}_2\text{O}_3$  content from 0.28 to 0.36 wt% can be attributed to the enhancement in  $\mu_i$  (see Fig. 4a), as the  $P_{\text{h}}$  is known to decrease with increasing  $\mu_i$ . However, as the  $\text{Co}_2\text{O}_3$  content is further increased to 0.44 wt%,  $P_{\text{cv}}$  at the three operating conditions is dramatically increased. The increase of  $P_{\text{cv}}$  as  $\text{Co}_2\text{O}_3$  content exceeds 0.36 wt% can be attributed to the increase of both  $P_{\text{h}}$  and  $P_{\text{e}}$ . The increase of  $P_{\text{h}}$  is due to the reduction of  $\mu_i$  (shown in Fig. 4a) and the increase of  $P_{\text{e}}$  is due to the reduction of  $\rho$  (shown in Fig. 7a).  $\text{Co}_2\text{O}_3$  content is increased from 0.36 to 0.44 wt%. Figure 8b–d show the temperature dependence of  $P_{\text{cv}}$  of MnZn ferrite with various  $\text{Co}_2\text{O}_3$  content at 100 kHz/200mT, 200 kHz/125mT, and 300 kHz/100mT, respectively. As directly shown in Fig. 7b, the resistivity of the MnZn ferrites with various  $\text{Co}_2\text{O}_3$  content dramatically decreases with increasing temperature. As a result, the eddy current loss of MnZn ferrites with various  $\text{Co}_2\text{O}_3$  is raised by increasing temperature. However, as the temperature is increased from 25 °C to the region of 40 ~ 80 °C,  $P_{\text{cv}}$  of the MnZn ferrites is reduced. This is due to the reduction of  $P_{\text{h}}$ , which is a result of  $\mu_i$  increasing to the maximum (shown in Fig. 5).

## 4 Conclusions

This study investigates the effects of  $\text{Co}_2\text{O}_3$  addition on the soft magnetic properties and loss performance of the MnZn ferrites used for power applications in the frequency range of 100–300 kHz. The saturation

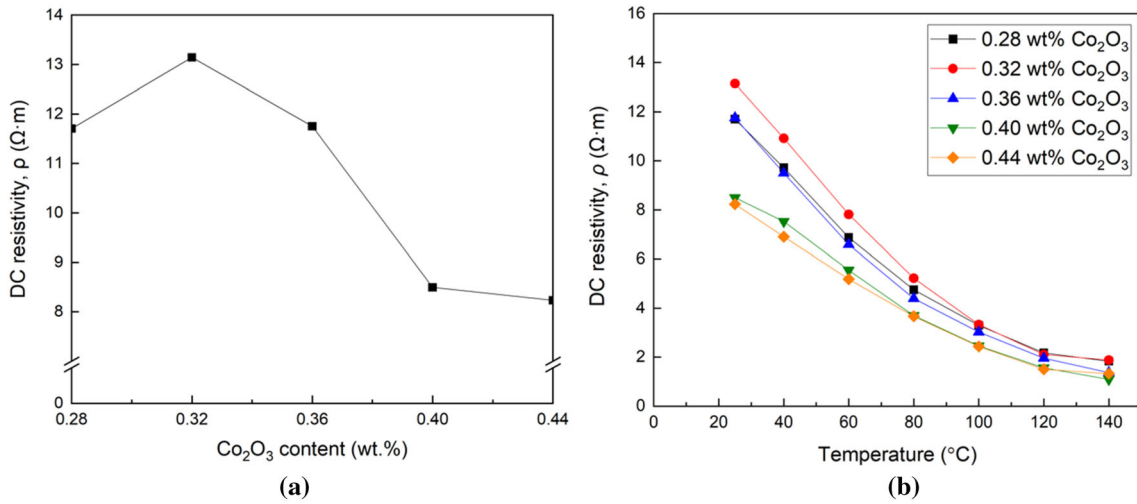


**Fig. 7** The DC resistivity ( $\rho$ ) of MnZn ferrites at room temperature and its temperature dependence change with the amount of  $Co_2O_3$  doping

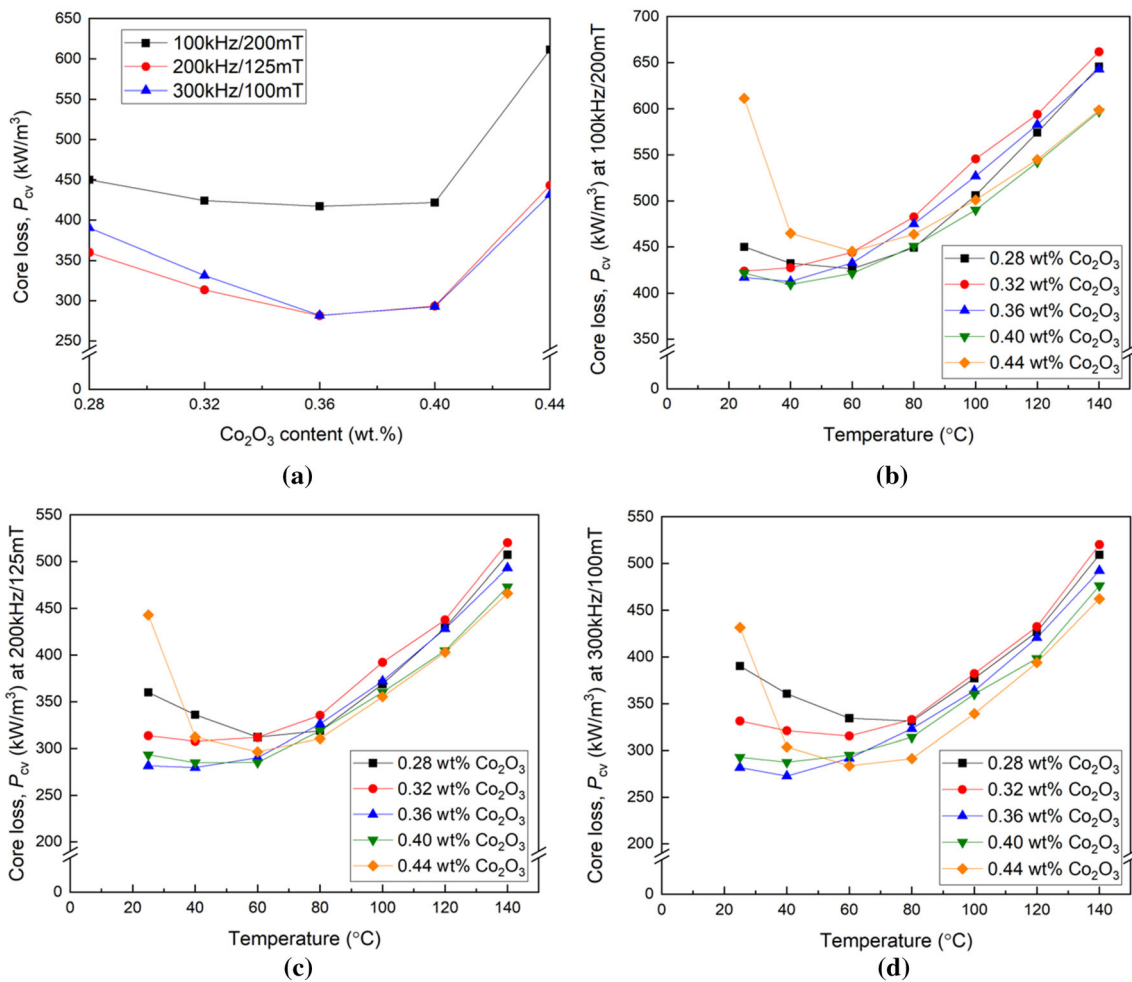


**Fig. 8** a The core loss ( $P_{cv}$ ) of MnZn ferrite at room temperature changing with  $Co_2O_3$  content. The temperature dependence of  $P_{cv}$  of MnZn ferrites with various  $Co_2O_3$  content at b 100 kHz/200mT, c 200 kHz/125mT, and d 300 kHz/100mT from 25 to 140  $^{\circ}C$

magnetization and density of the MnZn ferrites are slightly affected by the  $\text{Co}_2\text{O}_3$  doping. The initial permeability is seen to increase to a maximum of 2691 with a  $\text{Co}_2\text{O}_3$  addition of 0.36 wt%. The enhancement in the initial permeability corresponds to the minimum magnetic anisotropy value of  $16.85 \times 10^3 \text{ J/m}^3$ , which is attributed to the compensation effect on magnetocrystalline anisotropy brought about by the  $\text{Co}_2\text{O}_3$  addition. The DC resistivity of MnZn ferrites generally decreases with the increasing  $\text{Co}_2\text{O}_3$  content. In terms of the loss performance, proper amount of  $\text{Co}_2\text{O}_3$  doping at 0.36 wt% is seen to benefit the reduction of core loss, which is primarily the results of enhanced initial permeability. Due to the decreasing resistivity of MnZn ferrites with increasing temperature, the core loss generally increases as the temperature is increased from 25 to 140 °C. The minimum core loss appears in the temperature range of 40–80 °C, which corresponds to the temperature dependence of initial permeability.

### Author contributions

BF: Conceptualization, Formal analysis and Writing—Review and editing. YY: Investigation, Methodology, Formal analysis and Writing—Original draft. ZL: Investigation, Formal analysis and Writing—Original draft, review and editing. ZY: Conceptualization, Supervision, Project administration, Methodology, Writing—Review and editing. CW: Funding acquisition and Writing—Review. KS: Writing—Review. XJ: Writing—Review. QL: Funding acquisition and Writing—Review. ZL: Writing—Review.

### Funding

This present work was financially supported by the National Natural Science Foundation of China under Grant No. 52002055, and 52172267, the Sichuan Science and Technology Planning Project [2021YJ0556], the Innovation Group Project of Sichuan Province [2022JDTD0018], and the Science and Technology Bureau of Longquanyi District of Chengdu under Application Basis R&D Project No. LQXKJ-KJXM-2022-05.

### Data availability

All data generated in this study are reflected in the figures embedded in the article and can be made available on reasonable request.

### Declarations

**Conflict of interest** The authors declare that they have no known competing financial interests or personal relationships that could have appeared to influence the work reported in this paper.

### References

1. A. Lidow, M. De Rooij, J. Strydom, D. Reusch, J. Glaser, *GaN transistors for efficient power conversion* (Wiley, Hoboken, 2019)
2. Z. Zheng, S. Li, K. Peng, Magnetic properties regulation and loss contribution analysis of FeSi soft magnetic composites doped by carbonyl iron powders. *J. Magn. Magn. Mater.* **568**, 170423 (2023)
3. B.D. Cullity, C.D. Graham, *Introduction to magnetic materials* (Wiley, Hoboken, 2009)
4. R. Morineau, M. Paulus, Oxygen partial pressures of Mn-Zn ferrites. *Phys. Status Solidi (a)*. **20**, 373–380 (1973)
5. A. Znidarsic, M. Drogenik, Influence of oxygen partial pressure during sintering on the power loss of MnZn ferrites. *IEEE Trans. Magn.* **32**, 1941–1945 (1996)
6. K. Sun, Z. Lan, Z. Yu, Z. Xu, X. Jiang, Z. Wang, Z. Liu, M. Luo, Temperature and frequency characteristics of low-loss MnZn ferrite in a wide temperature range. *J. Appl. Phys.* **109**, 106103 (2011)
7. G. Wu, Z. Yu, Z. Tang, K. Sun, R. Guo, X. Zou, X. Jiang, Z. Lan, Effect of  $\text{CaCO}_3$  and  $\text{V}_2\text{O}_5$  composite additives on the microstructure and magnetic property of MnZn ferrites. *IEEE Trans. Magn.* **54**, 1–7 (2018)
8. G. Wu, Z. Yu, K. Sun, R. Guo, H. Zhang, X. Jiang, C. Wu, Z. Lan, Ultra-low core losses at high frequencies and temperatures in MnZn ferrites with nano- $\text{BaTiO}_3$  additives. *J. Alloys Compd.* **821**, 153573 (2020)
9. F. Xu, D. Zhang, G. Wang, H. Zhang, Y. Yang, Y. Liao, L. Jin, Y. Rao, J. Li, F. Xie, Densification and magnetic properties of NiCuZn low-sintering temperature ferrites with  $\text{Bi}_2\text{O}_3$ - $\text{Nb}_2\text{O}_5$  composite additives. *J. Alloys Compd.* **776**, 954–959 (2019)
10. K. Sun, Z. Lan, Z. Yu, L. Li, J. Huang, X. Zhao, Grain growth, densification and magnetic properties of NiZn ferrites with  $\text{Bi}_2\text{O}_3$  additive. *J. Phys. D* **41**, 235002 (2008)



11. Q. Luo, H. Su, X. Tang, Z. Xu, Y. Li, Y. Jing, Effects of Bi<sub>2</sub>O<sub>3</sub> addition on power loss characteristics of low-temperature-fired NiCuZn ferrites. *Ceram. Int.* **44**, 16005–16009 (2018)
12. S.E. Shirsath, Y. Yasukawa, A. Ghasemi, X. Liu, A. Morisako, Bi<sub>2</sub>O<sub>3</sub> liquid phase assisted and mn substituted permeability and magnetic properties of Ni-Cu-Zn ferrite for multilayer chip inductor application. *J. Appl. Phys.* **115**, 17A515 (2014)
13. H. Su, H. Zhang, X. Tang, Y. Jing, Effects of MoO<sub>3</sub> and WO<sub>3</sub> additives on densification and magnetic properties of highly permeable NiCuZn ferrites. *Mater. Chem. Phys.* **102**, 271–274 (2007)
14. O. Mirzaee, A. Shafyei, M.A. Golozar, H. Shokrollahi, Influence of MoO<sub>3</sub> and V<sub>2</sub>O<sub>5</sub> co-doping on the magnetic properties and microstructure of a Ni-Zn ferrite. *J. Alloys Compd.* **461**, 312–315 (2008)
15. K. Ono, S. Fukunaga, Y. Matsuo, Mn-Zn ferrite with MoO<sub>3</sub> and other oxide additives. *Trans. Magn.* **35**, 3406–3408 (1999)
16. D. Hu, F. Zhao, L. Miao, Z. Zhang, Y. Wang, H. Cheng, Y. Han, M. Tian, H. Gu, R. Ma, Magnetic properties and microstructures of a Ni-Zn ferrite ceramics co-doped with V<sub>2</sub>O<sub>5</sub> and MnCO<sub>3</sub>. *Ceram. Int.* **45**, 10028–10034 (2019)
17. B. Parvatheeswara Rao, C.-O. Kim, C. Kim, Influence of V<sub>2</sub>O<sub>5</sub> additions on the permeability and power loss characteristics of Ni-Zn ferrites. *Mater. Lett.* **61**, 1601–1604 (2007)
18. J.S. Lee, J.M. Cha, H.Y. Yoon, J.K. Lee, Y.K. Kim, Magnetic multi-granule nanoclusters: a model system that exhibits universal size effect of magnetic coercivity. *Sci. Rep.* **5**, 1–7 (2015)
19. C. Wu, W. Wang, Q. Li, M. Wei, Q. Luo, Y. Fan, X. Jiang, Z. Lan, Z. Jiao, Y. Tian, Barium hexaferrites with narrow ferromagnetic resonance linewidth tailored by site-controlled Cu doping. *J. Am. Ceram. Soc.* **105**, 7492–7501 (2022)
20. Q. Li, Y. Chen, C. Yu, L. Young, J. Spector, V.G. Harris, Emerging magnetodielectric materials for 5G communications: 18H hexaferrites. *Acta Mater.* **231**, 117854 (2022)
21. Z. Li, Y. Yi, H. Wang, Z. Yu, C. Wu, H. Dou, Q. Li, K. Sun, X. Jiang, Z. Lan, The effects of barium strontium titanate (BST) on the soft magnetic properties and loss performance of MnZn ferrites. *Ceram. Int.* **49**, 19631–19640 (2023)
22. W.D. Yang, Y.G. Wang, Effects of TiO<sub>2</sub> and Co<sub>2</sub>O<sub>3</sub> combination additions on the elemental distribution and electromagnetic properties of Mn-Zn power ferrites. *J. Magn. Magn. Mater.* **384**, 13–17 (2015)
23. K. Jiang, K. Li, C. Peng, Y. Zhu, Effect of multi-additives on the microstructure and magnetic properties of high permeability Mn-Zn ferrite. *J. Alloys Compd.* **541**, 472–476 (2012)
24. S.-F. Wang, Y.-J. Chiang, Y.-F. Hsu, C.-H. Chen, Effects of additives on the loss characteristics of Mn-Zn ferrite. *J. Magn. Magn. Mater.* **365**, 119–125 (2014)
25. K. Ohta, Magnetocrystalline anisotropy and magnetic permeability of Mn-Zn-Fe ferrites. *J. Phys. Soc. Japan* **18**, 685–690 (1963)
26. A. Fujita, S. Gotoh, Temperature dependence of core loss in co-substituted MnZn ferrites. *J. Appl. Phys.* **93**, 7477–7479 (2003)
27. Y. Ying, X. Xiong, N. Wang, J. Zheng, J. Yu, W. Li, L. Qiao, W. Cai, J. Li, H. Huang, Low temperature sintered MnZn ferrites for power applications at the frequency of 1 MHz. *J. Eur. Ceram. Soc.* **41**, 5924–5930 (2021)
28. A.D. Giles, F.F. Westendorp, The effect of cobalt substitutions on some properties of manganese zinc ferrites. *J. Phys. D* **9**, 2117 (1976)
29. V.T. Zaspalis, V. Tsakaloudi, M. Kolenbrander, The effect of dopants on the incremental permeability of MnZn-ferrites. *J. Magn. Magn. Mater.* **313**, 29–36 (2007)
30. A. Lucas, R. Lebourgeois, F. Mazaleyrat, E. Labouré, Temperature dependence of core loss in cobalt substituted Ni-Zn-Cu ferrites. *J. Magn. Magn. Mater.* **323**, 735–739 (2011)
31. H. Zhang, D. Zeng, Z. Liu, The law of approach to saturation in ferromagnets originating from the magnetocrystalline anisotropy. *J. Magn. Magn. Mater.* **322**, 2375–2380 (2010)
32. E.C. Devi, I. Soibam, Law of approach to saturation in Mn-Zn ferrite nanoparticles. *J. Supercond. Nov. Magn.* **32**, 1293–1298 (2019)
33. C. Rey, *Superconductors in the power grid: materials and applications* (Elsevier, Amsterdam, 2015)
34. X. Wang, S. Yi, C. Wu, G. Bai, M. Yan, Correlating the microstructure and magnetic properties of MnZn power ferrites via Co<sub>2</sub>O<sub>3</sub> and MoO<sub>3</sub> co-doping for MHz applications. *J. Magn. Magn. Mater.* **538**, 168324 (2021)
35. A. Sarikhani, L. Avazpour, W. Liyanage, R. Florez, E. Bohannan, D. Satterfield, M. Nath, J.E. Medvedeva, San Hor, transparency and room temperature ferromagnetism in diluted magnetic polycrystalline Zn<sub>1-x</sub>Cr<sub>x</sub>Te non-oxide II-VI semiconductor compounds. *J. Alloys Compd.* **924**, 166478 (2022)
36. A. Manzoor, M.A. Khan, T. Alshahrani, M.H. Alhossainy, M. Sharif, T. Munir, M.I. Arshad, M.A. Iqbal, Effect of Ho<sup>3+</sup> ions on microwave losses and high-temperature electrical behavior of Li-based magnetic oxides. *Ceram. Int.* **47**, 4633–4642 (2021)

**Publisher's Note** Springer Nature remains neutral with regard to jurisdictional claims in published maps and institutional affiliations.

Springer Nature or its licensor (e.g. a society or other partner) holds exclusive rights to this article under a publishing agreement with the author(s) or other rightsholder(s); author self-archiving of the accepted manuscript version of this article is solely governed by the terms of such publishing agreement and applicable law.